2D back-side diffraction grating for improved light trapping in thin silicon solar cells

Jo Gjessing,[1,2,3*] Erik Stensrud Marstein,[1,4] and Aasmund Sudbø[4,2]

[1] *Institute for Energy Technology, Pb 40, 2027 Kjeller, Norway*
[2] *University Graduate Center at Kjeller, Norway*
[3] *University of Oslo, Department of physics, Norway*
[4] *University of Oslo, Faculty of Mathematics and Sciences, Norway*
**jo.gjessing@ife.no*

Abstract: Light-trapping techniques can be used to improve the efficiency of thin silicon solar cells. We report on numerical investigation of a light trapping design consisting of a 2D back-side diffraction grating in combination with an aluminum mirror and a spacing layer of low permittivity to minimize parasitic absorption in the aluminum. The light-trapping design was compared to a planar reference design with antireflection coating and back-side aluminum mirror. Both normally and obliquely incident light was investigated. For normal incidence, the light trapping structure increases the short circuit current density with 17% from 30.4 mA/cm^2 to 35.5 mA/cm^2 for a 20 µm thick silicon solar cell. Our design also increases the current density in thinner cells, and yields higher current density than two recently published designs for cell thickness of 2 and 5 µm, respectively. The increase in current may be attributed to two factors; increased path length due to in-coupling of light, and decreased parasitic absorption in the aluminum due to the spacing layer.

OCIS codes: (050.1950) Diffraction gratings; (350.6050) Solar energy.

References and links

1. F. Henley, A. Lamm, S. Kang, and L. Tian, "Direct film transfer (DFT) technology for kerf-free silicon wafering," Proc. 23rd PVSEC, Valencia Spain, 1090–1093 (2008).
2. J. Nelson, *The Physics of Solar Cells,* (Imperial College Press, London, 2003).
3. E. Yablonovitch, "Statistical ray optics," J. Opt. Soc. Am. **72**(7), 899–907 (1982).
4. J. M. Gee, "Optically enhanced absorption in thin silicon layers using photonic crystals," Twenty-Ninth IEEE Photovolt. Spec. Conf., 150–153 (2002).
5. P. Sheng, A. N. Bloch, and R. S. Stepleman, "Wavelength-selective absorption enhancement in thin-film solar cells," Appl. Phys. Lett. **43**(6), 579–581 (1983).
6. C. Heine, and R. H. Morf, "Submicrometeer gratings for solar energy applications," Appl. Opt. **34**(14), 2476–2482 (1995).
7. M. T. Gale, B. Curtis, H. Kiess, and R. H. Morf, "Design and fabrication of submicron structures for light trapping in silicon solar cells," Proc. SPIE **1272**, 60–66 (1990).
8. H. Sai, H. Fujiwara, and M. Kondo, "Back surface reflectors with periodic textures fabricated by self-ordering process for light trapping in thin-film microcrystalline silicon solar cells," Sol. Energy Mater. Sol. Cells **93**(6-7), 1087–1090 (2009).
9. H. Sai, H. Fujiwara, M. Kondo, and Y. Kanamori, "Enhancement of light trapping in thin-film hydrogenated microcrystalline Si solar cells using back reflectors with self-ordered dimple pattern," Appl. Phys. Lett. **93**(14), 143501 (2008).
10. H. Sai, Y. Kanamori, K. Arafune, Y. Ohshita, and M. Yamaguchi, "Light trapping effect of submicron surface textures in crystalline Si solar cells," Prog. Photovoltaics **15**(5), 415–423 (2007).
11. R. Dewan, and D. Knipp, "Light-trapping in thin-film silicon solar cells with integrated diffraction grating," J. Appl. Phys. **106**(7), 074901 (2009).
12. A. Čampa, J. Krč, F. Smole, and M. Topič, "Potential of diffraction gratings for implementation as a metal back reflector in thin-film silicon solar cells," Thin Solid Films **516**(20), 6963–6967 (2008).
13. L. Zeng, Y. Yi, C. Hong, J. Liu, N. Feng, X. Duan, L. C. Kimerling, and B. A. Alamariu, "Efficiency enhancement in Si solar cells by textured photonic crystal back reflector," Appl. Phys. Lett. **89**(11), 111111 (2006).

#119649 - $15.00 USD Received 6 Nov 2009; revised 24 Feb 2010; accepted 24 Feb 2010; published 3 Mar 2010

14. N.-N. Feng, J. Michel, L. Zeng, J. Liu, C.-Y. Hong, L. C. Kimerling, and X. Duan, "Design of Highly Efficient Light-Trapping Structures of Thin-Film Crystalline Silicon Solar Cells," IEEE Trans. Electron. Dev. **54**(8), 1926–1933 (2007).
15. P. Bermel, C. Luo, L. Zeng, L. C. Kimerling, and J. D. Joannopoulos, "Improving thin-film crystalline silicon solar cell efficiencies with photonic crystals," Opt. Express **15**(25), 16986–17000 (2007).
16. D. Zhou and R. Biswas, "Harvesting photons in thin film solar cells with photonic crystals," Mater. Res. Soc. Symp. Proc. **1101**, (2008).
17. J. G. Mutitu, S. Shi, C. Chen, T. Creazzo, A. Barnett, C. Honsberg, and D. W. Prather, "Thin film solar cell design based on photonic crystal and diffractive grating structures," Opt. Express **16**(19), 15238–15248 (2008).
18. C. Haase, and H. Stiebig, "Optical Properties of Thin-film Silicon Solar Cells with Grating Couplers," Prog. Photovoltaics **14**(7), 629–641 (2006).
19. C. Haase, and H. Stiebig, "Thin-film silicon solar cells with efficient periodic light trapping texture," Appl. Phys. Lett. **91**(6), 061116 (2007).
20. F.-J. Haug, T. Söderström, M. Python, V. Terrazzoni-Daudrix, X. Niquille, and C. Ballif, "Development of micromorph tandem solar cells on flexible low-cost plastic substrates," Sol. Energy Mater. Sol. Cells **93**(6-7), 884–887 (2009).
21. J. Gjessing, E. S. Marstein, and A. Sudbø, "Modelling of light trapping in thin silicon solar cells with back side dielectric diffraction grating," Proc. 24th PVSEC, Hamburg Germany, 2604–2607 (2009).
22. http://software.kjinnovation.com/GD-Calc.html
23. L. Li, "Formulation and comparison of two recursive matrix algorithms for modeling layered diffraction gratings," J. Opt. Soc. Am. A **13**(5), 1024–1035 (1996).
24. http://ab-initio.mit.edu/meep/
25. A. Taflove, and S. C. Hagness, *Computational Electrodynamics: The Finite-Difference Time-Domain Method*, (Artech House Publishers, Norwood MA, 2005).
26. J. D. Joannopoulos, S. G. Johnson, J. N. Winn, and R. D. Meade, *Photonic Crystals: Molding the Flow of Light*, (Princeton University Press, New Jersey 2008).
27. C. M. Herzinger, B. Johs, W. McGahan, J. Woollam, and W. Paulson, "Ellipsometric determination of optical constants for silicon and thermally grown silicon dioxide via a multi-sample, multi-wavelength, multi-angle investigation," J. Appl. Phys. **83**(6), 3323–3336 (1998).
28. E. D. Palik ed., *Handbook of Optical Constants of Solids*, (Academic Press, San Diego, 1985).
29. http://rredc.nrel.gov/solar/spectra/am1.5/
30. M. A. Green, *Silicon Solar Cells – Advanced principles and practice*, (Centre for Photovoltaic Devices and Systems, Sydney, 1995).
31. H. A. Macleod, *Thin-Film Optical Filters*, (Institute of Physics Publishing, Bristol, 2001).
32. C. H. Henry, "Limiting efficiencies of ideal single and multiple energy gap terrestrial solar cells," J. Appl. Phys. **51**(8), 4494–4500 (1980).
33. E. Schneiderlöchner, R. Preu, R. Lüdemann, and S. W. Glunz, "Laser-Fired Rear Contacts for Crystalline Silicon Solar Cells," Prog. Photovoltacis **10**, 29–34 (2002).
34. http://www.mathworks.com/

1. Introduction

The cost per watt of solar cells needs to be reduced for solar electricity to become competitive with energy produced from fossil fuels. Thinner cells can reduce both the amount of material needed, and also demand on material quality, thereby reducing both production costs and energy consumption. Thin film technologies aim at reducing cost through decreased material consumption, but deposited thin film solar cells have inferior efficiency compared to the much thicker wafer based crystalline silicon (Si) cells. Recent discoveries have showed that it is also possible to make high quality crystalline Si substrates and solar cells with thickness down to 20 μm and below [1]. Although this approach holds much promise, one fundamental challenge must be overcome. Si exhibits an indirect band gap, and at this thickness a significant part of the light is lost due to insufficient absorption of the near infrared radiation. Thus, the decrease in cost obtained by using very thin Si substrates is offset by a decrease in efficiency. In order to avoid excessive optical losses, thin Si cells therefore need an efficient light-trapping scheme.

For monocrystalline Si the most common method in the industry today is alkaline anisotropic wet etching, which results in a random structure of pyramids [2]. This works well for [100] oriented wafers, but it is not as effective for the [111] orientation. This might pose a problem for wafers made by the technology used in [1] where wafers are [111] oriented. For multicrystalline Si, the use of isotropic acidic etches is more common. Especially the alkaline etching of monocrystalline Si has proved successful for front side light trapping. Both methods results in fairly large surface structures with sizes in the order of 2-10 μm. For deposited thin film Si cells, glass materials with textured transparent oxide coatings, are

#119649 - $15.00 USD Received 6 Nov 2009; revised 24 Feb 2010; accepted 24 Feb 2010; published 3 Mar 2010

popular substrates due to their potential for light trapping. These random structures have dimensions below 1 μm. Yablonovitch [3] showed that an ideal patterning with random total internal reflection, in the statistical limit would enhance absorption by $4n^2$, where n is the refractive index of the material ($4n^2$~50 for Si). However, it is not known whether nor how such ideal patterns can be fabricated.

Periodic structures have the potential of achieving better light trapping than random structures over a limited spectral range [4,5]. Periodic structures for light trapping in solar cells has been investigated earlier [5–7], and also in a number of recent works [8–19]. One type of such gratings is diffraction gratings made of metal. Such gratings are relative simple to fabricate. However, a problem with metal gratings is that they general suffer from strong narrowband absorption lines [7,12]. To overcome this problem, pure dielectric designs combining gratings and back reflectors made from Bragg stacks, have been proposed [13–17]. Zeng et al. [13] achieved good correspondence between the theoretical predictions and the measured short circuit current for a 5 μm thick c-Si solar cell. Low-cost fabrication of periodic structures has also been investigated. Haug et al. [20] made 2D structures on a low-cost substrate using hot embossing, while Sai et al. [8,9] has demonstrated a self ordered periodic structured back reflector with periods as small as 300 nm. With a period of 900 nm these structures showed better light-trapping properties than the Asahi U-type glass. The Asahi U-type glass is a state-of-the-art random texturing for thin-film solar cells. Most of the literature on the subject focuses on thin cells in the range of 0.5-5 μm. The effect of back-side light-trapping structures will in general be most prominent for such thin cells, due to low baseline absorption. Thicker cells on the other hand, will have the advantage that the solar spectrum that reaches the back side is more narrow-banded, which is an apparent advantage for periodic structures.

In [21] we presented a 2D-periodic back-side grating structure that combined a purely dielectric grating with a flat Al reflector, separated from the grating by a layer of SiO_2. The low refractive index of SiO_2 provides a large index contrast which gives the diffraction grating a spectrally broad response. Admittedly, air provides an even larger index contrast, but is impractical. In addition to reducing parasitic absorption in the Al, the oxide layer provides excellent surface passivation, a vital prerequisite for any highly efficient, thin, crystalline Si solar cell. High quality back-side surface passivation is especially important for thin cells where carrier excitation to a greater extent will occur close to the back side. In this paper we go into further details of the properties of the structure, and perform an optimization of the vital parameters grating period, fill factor, grating thickness and oxide thickness. We have also investigated how oblique incidence angle affects the light trapping properties. We focus in this work on a Si thickness of 20 μm, which is particularly relevant in the light of the recent findings of Henley et al. [1].

2. Numerical methods

To accurately predict the response of the back-side diffraction grating, rigorous electromagnetic modelling of the light is needed. Numerical modelling was performed with Grating Diffraction Calculator (GD-Calc) [22], a software package that uses rigorously coupled wave analysis (RCWA) [23]. GD-Calc is a fully vectorial solver and solves the Maxwell equations for a single frequency. The results from GD-Calc have been compared with results obtained with the software package Meep [24]. Meep uses the method of finite difference time domain (FDTD) [25,26] for solving the Maxwell equations numerically. Both methods (RCWA and FDTD) showed almost identical results for non-absorbing materials. However, with RCWA it is straightforward to analyze the strength of each diffraction order separately. This is imperative when analyzing the grating efficiency. Finally, RCWA is also better suited when the model structure contains layers with large differences in thickness.

There are at least two limiting cases that can be accurately described by simple scalar models for the propagation of light. These cases do not give us quantitative information about the light trapping design, but we have found the fast calculations allowed by the scalar models to be very useful in limiting the number of time-consuming RCWA simulations needed to do

#119649 - $15.00 USD Received 6 Nov 2009; revised 24 Feb 2010; accepted 24 Feb 2010; published 3 Mar 2010

the design. The fast calculations have allowed us to limit the size of the four-dimensional volume in parameter space that we had to map using RCWA simulations.

Figure 1 shows the structure that was modeled in GD-Calc. This structure has been compared with a reference model with equal thickness (e.g. 20 μm), single-layer AR coating, and a planar back-side Al mirror. Wavelength-dependent refractive index data (real and imaginary part) is used for absorbing materials (i.e. Si [27], Al and Ag [28]), while a refractive index of 1.5 and 1.95 is used for SiO_2 and Si_3N_4 respectively. The Si_3N_4 AR layer was designed to give a minimum reflectance at a wavelength just above 600 nm, which corresponds to a thickness of 78 nm.

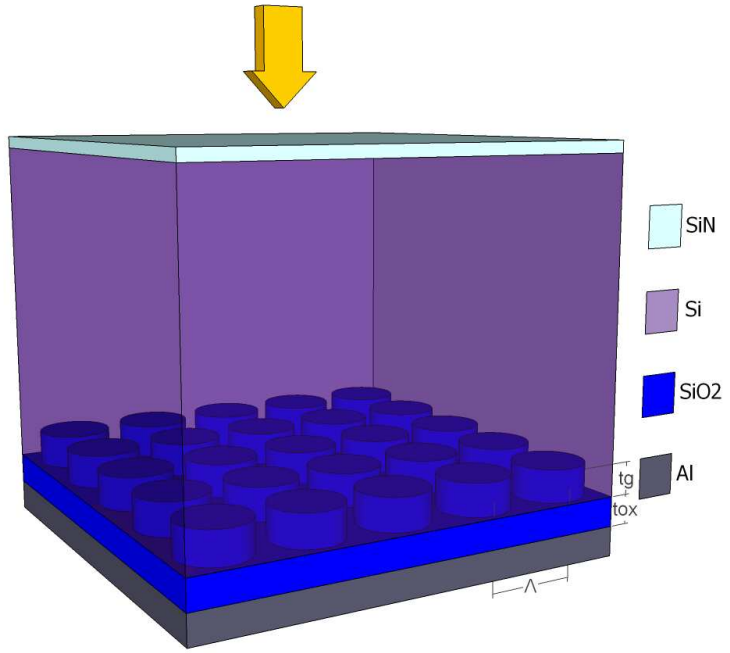

Fig. 1. Optical solar cell model structure used in the computations (not to scale). A single layer of Si_3N_4 is used as AR-coating. The reference structure is similar except that the SiO_2 and the grating layer are removed, and the Si is in direct contact with a planar Al-mirror.

A quantitative measure is needed for comparison of the different design parameters. The parameters as indicated in Fig. 1 are the grating period Λ, grating thickness t_g, thickness of the oxide layer t_{ox} and fill factor, here defined as the area covered by holes divided by the total area. A suitable measure of the performance of the structure is the short circuit current density (J_{sc}) excited by the AM 1.5 solar spectrum [29], which is calculated as shown in Eq. (1):

$$J_{sc} = q\int_0^\infty A(\lambda)\Phi(\lambda)\mathrm{d}\lambda \qquad (1)$$

Equation (1) provides a limit for the maximum J_{sc} that would be obtained if all the generated electron hole pairs reach the contacts. Here, λ is the wavelength in [nm], q the elementary charge in [C], $A(\lambda)$ the absorbance which is a dimensionless wavelength dependent factor between zero and one, calculated by GD-calc and $\Phi(\lambda)$ is the spectral density of the photon irradiance with dimension [$s^{-1}m^{-2}nm^{-1}$] from the AM1.5 spectrum normalized so that the irradiance equals 1000 W/m^2. The integration is performed from 0 to ∞ but $\Phi(\lambda)$ is negligible for λ<300 nm while $A(\lambda)$ is negligible for λ>1100 nm due to the bandgap of Si.

Absorption in the Al-mirror may be substantial, but does not contribute to J_{sc}. This parasitic absorption is therefore subtracted from the total absorption. The decoupling of parasitic absorption from the absorption in the rest of the cell is calculated in a straightforward

#119649 - $15.00 USD Received 6 Nov 2009; revised 24 Feb 2010; accepted 24 Feb 2010; published 3 Mar 2010

manner in GD-Calc. The absorption is calculated by taking the difference in Poynting vector going into and out of the given plane.

Free carrier absorption (fca) [30] is not considered in this model. As long as the Si is lightly doped, as is common in the bulk Si, fca will not make a big contribution for solar cell applications.

3. Grating analysis

3.1 Grating equation

The most important property of the grating is to increase the path length of light inside the Si by coupling the light into higher diffraction orders. The angles of the diffracted orders are given by the two-dimensional grating equation. We use the word grating in this article to describe our bi-periodic pattern of cylinders as shown in Fig. 1. The direction of the incident beam may be described by the polar angle θ, defined as the angle between the beam and the normal to the plane, and the azimuth angle φ, which determines the orientation in the plane. The outgoing beam may be diffracted in either direction of periodicity and will be characterized by two diffraction orders m_x and m_y. For each pair of diffraction orders (m_x, m_y), the corresponding beam angles θ, and φ for the diffracted beam are different.

For a one-dimensional (linear) grating and an angle of incidence in the plane of periodicity, the grating equation takes the form of Eq. (2). The two-dimensional grating equation is a straight forward extension of the one dimensional equation.

$$n_o \sin(\theta_m) = n_i \sin(\theta_i) + \frac{m\lambda}{\Lambda} \tag{2}$$

n is the refractive index, θ the angle between the beam and the normal to the plane in the direction of periodicity (classical mount), Λ the grating period, λ the free-space wavelength, and m the diffraction order. m is also the subscript of the angle θ_m of the diffracted wave corresponding to diffraction order m. The incident beam and material have the subscript i while the outgoing material has the subscript o. In this case we have diffraction in Si, so that $n_i = n_o \approx 3.6$. From Snell's low of refraction, the critical angle where total internal reflection will occur at a Si-air boundary is $\theta_c = \sin^{-1}(1/n_{Si}) \sim 16$ degrees. Light from the Si incident at the Si-air boundary at a larger angle will be totally internally reflected back into the Si. Adding layers of other materials between the Si and air does not change the critical angle for escape into the air.

From Eq. (2) we see that at normal incidence ($\theta_i = 0$) the angle of the diffracted beam is given by $\sin(\theta_m) = m\lambda/(n\Lambda)$. For small periods (i.e. $\Lambda < \lambda/n$) the equation has a real solution only for the zeroth order ($m=0$), i.e. specular reflectance. If the period is larger than the wavelength of light, the angle of the lower diffraction orders will become too small to efficiently increase the path length, and the lowest diffraction order will also lie in the escape cone of Si (~16 degrees). This limits the optimal grating period to the interval $\Lambda \in (\lambda / n_{Si}, \lambda)$.

Since the terrestrial solar spectrum contains a wide band of wavelengths we define a mean wavelength $\overline{\lambda}$ as shown in Eq. (3):

$$\overline{\lambda} = \frac{\int_0^\infty \lambda (A_{base}(\lambda) - A_{opt}(\lambda)) \Phi(\lambda) d\lambda}{\int_0^\infty (A_{base}(\lambda) - A_{opt}(\lambda)) \Phi(\lambda) d\lambda} \tag{3}$$

A_{base} is the absorbance of light through a slab of thickness L (i.e. [1-exp(−2α(λ)L]). The factor 2 in the exponential derives from assuming a perfect back-side reflector, which doubles the path length of the light. A_{opt} is the optimum absorbance given by the Yablonovitch limit [3] for the same thickness, so that the factor 2 is replaced by $4n_{Si}^2$. The light which is absorbed in an optimal cell, but is not absorbed in the baseline cell, is of most relevance when optimizing the periodic structure. Equation (3) gives a weighted distribution that goes to zero for both

#119649 - $15.00 USD Received 6 Nov 2009; revised 24 Feb 2010; accepted 24 Feb 2010; published 3 Mar 2010

short and long wavelengths, and with a $\bar{\lambda}$ of 0.98 μm for a 20 μm thick Si slab. For simplicity, an ideal AR-layer with zero reflectance is assumed in this calculation.

3.2 Diffraction efficiency

The diffraction angles may be found from the grating equation, but the power distributed in each diffraction order is a sensitive function of the grating thickness t_g. A convenient measure of the suitability of the grating for light trapping purposes is the power fraction diffracted into higher orders, D_{HO}, which is a dimensionless number between zero and one, defined in Eq. (4) in the same way as in [10]:

$$D_{HO} = \sum_{m_x=-\infty}^{m_x=\infty} \sum_{m_y=-\infty}^{m_y=\infty} D_{m_x m_y} - D_{00} \tag{4}$$

In order to calculate D_{HO}, a summation is done over all diffraction orders (m_x, m_y). Thereafter, the component in the zeroth order D_{00}, which represents specular reflection, is subtracted.

3.3 Large-period approximation

To maximize D_{HO}, the specular reflection power fraction D_{00} needs to be minimized. In the limit of a Λ much larger than λ, this is achieved by designing the grating thickness so that the reflection from the peaks and valleys of the grating interfere destructively. In a pure metal grating this is done by making the grooves $\lambda/4$ deep. In our design, however, the phase of the reflected light is dependent not only on the grating thickness t_g, but also upon the oxide thickness t_{ox}, which is the distance from the grating to the back-side Al-mirror. However, the principle of the $\lambda/4$ grating may be extended to the case of a multilayer structure by calculating the phase of the reflected wave from the peaks and valleys of the grating structure independently. The two phases can be calculated for two uniform multilayer slab structures, one representative for the peaks of the cylinders of Fig. 1, and the other representative of the space between the cylinders. For each slab structure, we used the method of transfer matrix [31] to calculate the phase of the reflected wave. This calculation is very much faster than an RCWA simulation.

3.4 Small-period (electrostatic) approximation

For small periods the light does not interact with the grating peaks and valleys independently. Instead, the EM-waves will behave as in a homogeneous material where the effective refractive index n_{eff} is determined by the distribution of the light between the low and the high dielectric. Thus, the phase of the light reflected from the grating structure behaves like the phase of the light reflected form a homogenous slab structure where the grating layer is replaced by a homogenous (so-called metamaterial) layer with an effective refractive index. Note that the grating structure will diffract light into higher orders as long as the period Λ is larger than λ/n_{Si}. Nevertheless we have found that we can use the small-period approximation to find the optimal grating thickness needed to minimize D_{00} also for Λ slightly larger than λ/n_{Si}. The thickness of the layers should be chosen so that the light reflected from the effective homogenous slab structure has a phase of π (or equivalently -π) relative to the top of the cylinders, referring to Fig. 1. With this condition satisfied D_{00} will be suppressed due to destructive interference. Again, the calculation of the effective refractive index of the metamaterials is much faster than an RCWA simulation.

4. Simulation results

4.1 Diffraction orders and phase plot

Figure 2 compares D_{HO} calculated with GD-Calc (a) as a function of t_g and t_{ox}, with the phase difference between grating peaks and valleys (b), as calculated for the large-period approximation explained above. The free space wavelength is 1 μm, while the period in the calculations with GD-Calc is 2 μm so it is closer to the large period regime than the small

#119649 - $15.00 USD Received 6 Nov 2009; revised 24 Feb 2010; accepted 24 Feb 2010; published 3 Mar 2010

period regime. The figure shows clear correlations between D_{HO}-maxima, and the parts of the phase plot where the phase difference is close to π (or equivalently -π). Increasing the period in GD-Calc to 5 μm gives an excellent correlation for the entire range of t_g, t_{ox} values shown in Fig. 2.

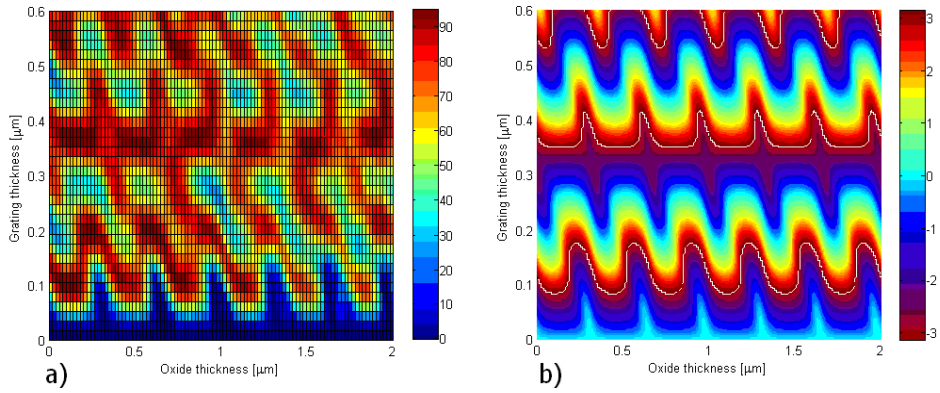

Fig. 2. Power fraction D_{HO} in higher-order diffracted beams (a), defined in Eq. (4) as a function of t_g and t_{ox} calculated with GD-calc using a period of 2 μm. (b) shows the phase difference between grating peaks and valleys calculated independently for the peaks and valleys by the transfer matrix method. A phase difference close to + π or -π indicates destructive interference at normal incidence, resulting in a corresponding maximum D_{HO}.

Figure 3 shows the small period case where the D_{HO} map (a) is calculated with a period of 0.3 μm (free-space wavelength of 1 μm), which is close to the minimum period that still allows higher diffraction orders to propagate in the Si superstrate. The phase map in Fig. 3(b) shows the reflected phase from a homogenous structure of layers where the grating layer is replaced by a slab of material with an effective refractive index n_{eff} of 3. We have written a Matlab [34] program to calculate the zero-frequency effective refractive index of a periodic pattern of parallel cylinders having the E-field perpendicular to the cylinder axes. We have used the standard angular harmonic solutions for Laplace's equation in cylindrical coordinates to set up a series expansion for the electric field, matched the electric field analytically at the surface of the cylinder, and imposed periodic boundary conditions by point matching of the electric field along the edges of a square unit cell. For this zero-frequency case we found a n_{eff} of 2.5 with a fill factor of 0.5. A general trend in the dispersion relation of the periodic structure is that the slope of the lowest band is reduced when the frequency increases. This corresponds to an increase in effective refractive index owing to accumulation of light in the dielectric with a high refractive index. Examples of such diagrams can be found in the book of Joannopoulos et a [26]. The discrepancy between the calculated value and the fitted value in Fig. 3(b) may be attributed to the fact that we are not comparing to a zero-frequency case. It is interesting to note that the grating structure has meta-material like properties also above the diffraction limit. For Λ between the two extreme cases, the D_{HO} map has features from both the small period phase map in Fig. 3 and the large period phase map in Fig. 2.

#119649 - $15.00 USD Received 6 Nov 2009; revised 24 Feb 2010; accepted 24 Feb 2010; published 3 Mar 2010

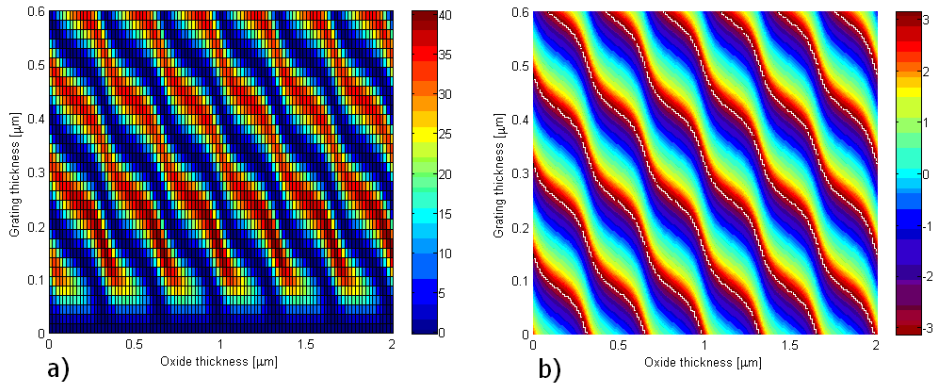

Fig. 3. (a) D_{HO} defined in Eq. (4) as a function of t_g and t_{ox} calculated with GD-calc using a period of 0.3 µm. Note that the magnitude of the higher order reflections is much lower than in figure Fig. 2(a). Figure 3(b) shows the phase plot of a reflected wave from a one dimensional stack of homogenous slabs where the grating layer have been substituted by a homogenous slab with an effective refractive index n_{eff} = 3. The calculation of phase is performed with the transfer matrix method.

The phase maps in Fig. 2(b) and Fig. 3(b) indicate the t_g and t_{ox} parameter space where we will expect to find D_{HO}-maxima. They also show us how the interactions between the layer thicknesses influence the positions of the maxima. However, the phase maps do not indicate the strength of the diffraction orders (as long as all phase maxima have the same phase e.g. ± π). In this case the analysis of the D_{HO} at the wavelength $\bar{\lambda}$ defined in Eq. (3) is a powerful tool. It provides the diffraction efficiency, and it can be performed without taking the 20 µm Si slab into account. The GD-calc simulations are faster without the slab on top. The presence of the slab with a thickness of many tens of wavelengths in the structure creates a need for a very fine wavelength sampling in every spectrum calculated, to be able to resolve the Fabry-Perot interference pattern from the 20-µm-thick Si slab. Correlation between the D_{HO}-map and absorption in the Si-slab is good, except that the D_{HO}-map seems to overestimate the light-trapping at shorter periods (not shown). To incorporate the effect of total internal reflections and secondary grating interactions simulations must be performed with the full model structure of Fig. 1.

4.2 Parasitic absorption

Al is the common choice as a back reflector for wafer based solar cells in industry today, mainly due to its low cost. However, Al reflectors suffer from a high absorption. Gratings may further enhance this problem by providing a means for coupling light to the reflector. To reduce parasitic absorption in the Al-mirror, we have placed a layer of SiO_2 between the grating and the Al mirror. Figure 4 shows the effect of t_{ox} on J_{sc} and parasitic J_{sc} (i.e. absorption current in the Al). We observe that the parasitic absorption in the Al, and therefore also the electric field strength in the Al, is only slightly effected by the thickness of the spacing layer for thicknesses above 0.2 µm. J_{sc} however continues to oscillate. This implies that it must be the *phase* of the light reflected from the Al that generates these oscillations. This is confirmed by seeing how the oscillations in J_{sc} match excellently with oscillations expected from Fabry-Perot interference in the oxide spacing layer. The same effect can also be seen in Fig. 2 and Fig. 3.

#119649 - $15.00 USD Received 6 Nov 2009; revised 24 Feb 2010; accepted 24 Feb 2010; published 3 Mar 2010

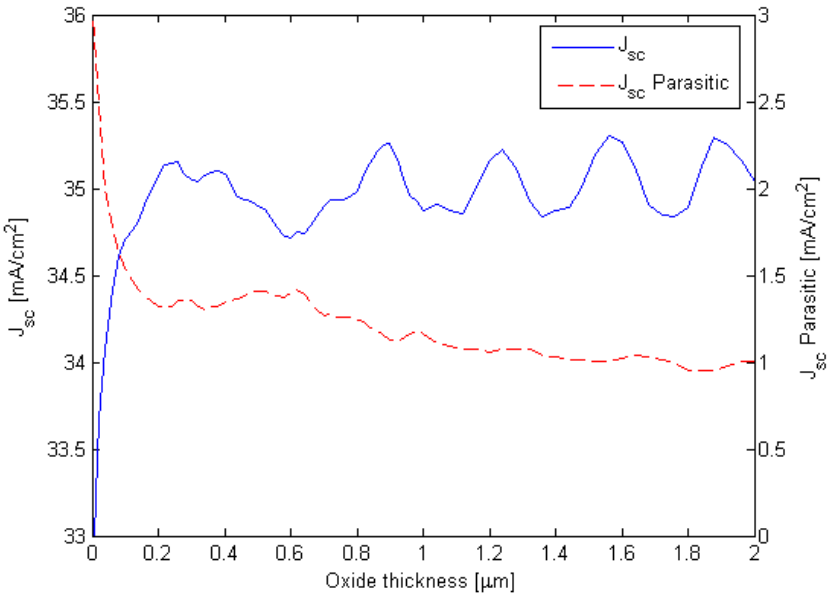

Fig. 4. The figure shows J_{sc} on the left axis, and parasitic absorption on the right axis as a function of thickness of the SiO_2 spacing layer t_{ox} between the grating and the Al mirror.

4.3 Short circuit current

Figure 5 displays a parameter scan over both Λ and fill factor for the full optical solar cell structure. A grating thickness t_g = 0.23 μm and spacing layer thickness t_{ox} = 0.2 μm was chosen on the basis of a D_{H0}–map similar to the ones shown in Fig. 2(a) and Fig. 3(a). We can see that highest values of J_{sc} are obtained over a broad parameter range with periods from 0.7 μm up to 1 μm. One should be aware that in general, for each t_g and t_{ox} we get a different version of Fig. 5, with different locations and values of the J_{sc} maxima. However, the highest J_{sc} values seem to be in the period range from around 0.6 μm to 1 μm also for other t_g and t_{ox} combinations (not shown). In addition, the trend that the ridges corresponding to high J_{sc} values moves towards higher period with increasing fill factor (most notable for small periods), remains the same also for other t_g and t_{ox} combinations. For thinner substrates Eq. (3) gives a smaller $\bar{\lambda}$, and the locations of the maxima in Fig. 5 will shift towards shorter periods.

#119649 - $15.00 USD Received 6 Nov 2009; revised 24 Feb 2010; accepted 24 Feb 2010; published 3 Mar 2010

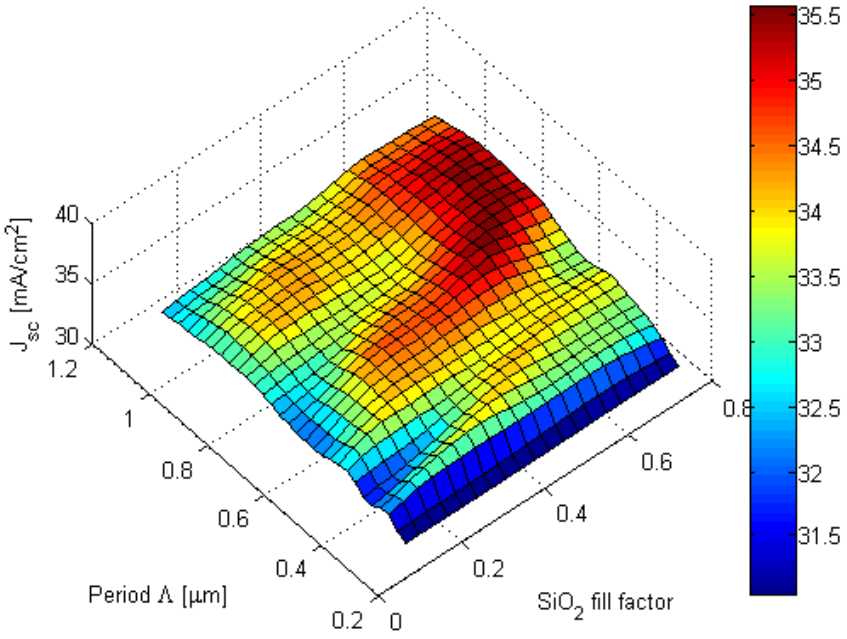

Fig. 5. The figure shows J_{sc} for different combinations of grating period Λ and fill factor for a grating thickness t_g = 0.23 μm and a spacing layer thickness t_{ox} = 0.2 μm.

For Λ outside the interval $\Lambda \in (\lambda / n_{Si}, \lambda)$ described earlier, J_{sc} drops significantly. For smaller periods J_{sc} drops because only the zeroth diffraction order remains and D_{OH} = 0. For periods larger than 1 μm there are still higher orders that may be diffracted at large angles, so the cut-off is not as sudden as the cut-off for small periods.

In Fig. 6 the spectral absorbance in the light-trapping structure from Fig. 1 is compared with the spectral absorbance in a reference cell having equal thickness and AR-coating, but a planar back side Al reflector. The figure shows a significant improvement in the wavelength range from 0.8 to 1.1 μm. At wavelengths below 0.7 μm there is no discernable difference in the absorption, and the front side reflectance is the limiting factor. Figure 6(a) shows the rapid Fabry-Perot oscillations resulting from interference in the 20 μm thick Si slab. A time-consuming dense wavelength sampling is required to resolve the oscillations. Analysis of the D_{HO} is therefore an efficient way to do a faster analysis of the structure. In Fig. 6(b) one can see remnants of these oscillations, after they have been reduced with the help of a digital low-pass filter (a moving average), for easier comparison of the curves.

#119649 - $15.00 USD Received 6 Nov 2009; revised 24 Feb 2010; accepted 24 Feb 2010; published 3 Mar 2010

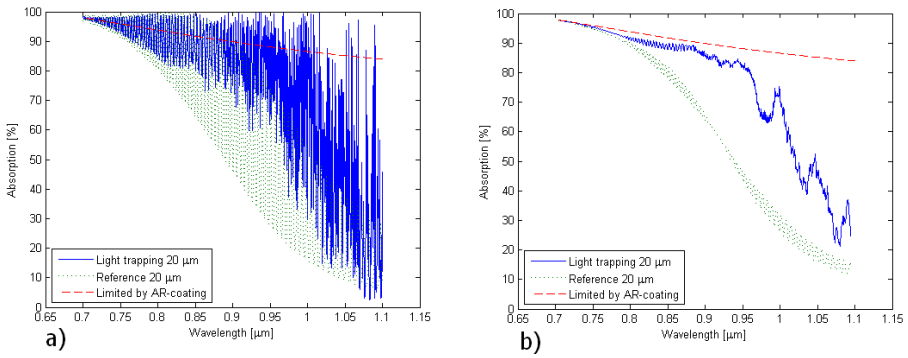

Fig. 6. The figure shows absorption as a function of wavelength for the light-trapping design (solid line) and the reference (dotted line), compared to the limitation imposed by the front-side reflectance from a single layer AR-coating on top of an infinite Si slab (dashed line). (a) shows the simulated spectral response, and (b) shows a moving average of the same data. A Λ of 0.7 µm, fill factor of 0.6, t_g of 0.23 µm and t_{ox} of 0.2 µm are used for the light trapping structure.

In Table 1 the absorbance in Fig. 6 is inserted in Eq. (1) to calculate the J_{sc}. We see that the light-trapping structure with Al reflector holds the potential to improve J_{sc} by 5.1 mA/cm^2, or 17% relative, compared to a 20 µm thick reference cell.

Table 1. Comparison of J_{sc} for different model structures assuming all excited charge carriers reach the contacts. The spectral response of the 20 µm reference and the light-trapping structure with Al-reflector is shown in Fig. 6. The same parameters are used for all light trapping three cells, varying only the back side reflector. The AM 1.5 absorbance is the percentage of the photons in the wavelength interval 300-1100 nm which are absorbed in the Si.

Structure	J_{sc} [mA/cm^2]	AM 1.5 absorbance
Light trapping 20 µm – ideal reflector	36.1	83.0%
Light trapping 20 µm – Ag reflector	35.9	82.5%
Light trapping 20 µm – Al reflector	35.5	81.6%
Reference 20 µm	30.4	69.9%
Reference 160 µm	36.6	84.1%

The reflectance of Ag is in general significantly better than for Al. Table 1 show us that we will gain 0.4 mA/cm^2 by replacing the Al reflector in Fig. 1 with Ag. Actually, the parasitic J_{sc} is reduced by 0.7 mA/cm^2 for the Ag reflector (not shown), but only a bit more than half of this is contributing to the J_{sc}. For a perfect reflector the J_{sc} reaches 36.1 mA/cm^2. The light-trapping cell with Al reflector from Table 1 actually achieves the same J_{sc} as a 5 times thicker planar reference cell with the same AR coating and an Al reflector. This is equivalent to an average absorption length of 180 µm in silicon, or an increase in optical thickness by a factor of 9. In other words, the number of photons absorbed in the light-trapping cell with an Al reflector is the same as what would be absorbed in the first 180 µm of an infinitely thick Si-slab with the same AR-coating as the light-trapping cell. The light-trapping structure with Ag reflector increases optical thickness by a factor of 11.

4.4 Comparison with literature

Comparison with different light-trapping concepts is not straight forward due to the differences in cell design, thickness, surface structures, and material and cell materials. To further complicate the picture, different authors use different parameters to describe the effect of their light-trapping design. Quantitative comparison of back-side light-trapping structures with AR-structures is unsuitable since the back-side structures address only the part of the solar spectrum that reaches the back side, while AR-structures address the whole solar spectrum. The predicted light-trapping effect in solar cells for periodic structures have been confirmed experimentally by other authors for 1D gratings [13,18]. No such comparison has

#119649 - $15.00 USD Received 6 Nov 2009; revised 24 Feb 2010; accepted 24 Feb 2010; published 3 Mar 2010

been found for 2D gratings. However, a 2D Al dimple pattern was recently compared to one of the best random structures available, and showed good results [9].

Most of the relevant data from literature focus on thinner cells. For comparison purposes we have modeled the light trapping response of our periodic structure on thinner cells. However, a separate optimization of AR-coating or grating parameters for the given thickness has not been performed. Therefore, a further improvement of light trapping could be expected from our structure by performing the optimization for the given thickness.

Mutitu et al. [17] found a J_{sc} of 30.3 mA/cm^2 for a 5 µm thick c-Si cell including both a 1D triangular shaped back-side grating with a dielectric Bragg reflector, and a front side binary grating with a double layer AR-coating. A J_{sc} of 27.4 mA/cm^2 was obtained with no front-side grating, and a binary grating together with the Bragg reflector on the back side. We obtain an equivalent J_{sc} (30.3 mA/cm^2) with a planer front-side AR-coating and our back-side structure. We observe that parasitic absorption in the Al-reflector has more than doubled at this thickness compared to the 20 µm cell. The use of Ag back reflector would be more advantageous at this thickness than for the 20 µm thick cell.

Bermel et al. [15] modeled a 2 µm c-Si cell with a dielectric Bragg back-reflector in combination with different types of periodic light scattering structures. Bermel used Henry's model [32] for radiative recombination as a loss mechanism, to get efficiency from J_{sc}. Bermel's best result was obtained for a 2D triangular back-side cylinders pattern, and showed an efficiency of 16.32% corresponding to a J_{sc} of 23.9 mA/cm^2 for a lossless model like ours. With our structure and the Al back reflector applied to a 2 µm thick cell we obtain a J_{sc} of 26.4 mA/cm^2, or an improvement of 10% over Bermel's structure.

4.5 Angular dependence

For non-tracking solar panels the angle of the incident light (i.e. the sun) varies with time. Thus, it is of great interest to study the response of the light-trapping structure at different incidence angles. The angle of incidence is in general specified by the polar angle θ and the azimuth angle φ. We have studied the effect of θ on the J_{sc} while keeping φ fixed so that the incidence plane is along one of the directions of periodicity. Both s-polarization and p-polarization are considered. For s-polarization the E-field is transverse to the normal of the layer structure, while for p-polarization the E-field is in the plane of incidence. The solar irradiance is unpolarized, thus the light incident at the solar cell contains equal amounts of s- and p-polarization. In real life, the solid angle captured by the module (as seen from the sun) decreases with $\cos(\theta)$. Small angles of incidence will therefore be relatively more important with respect to power generation than larger angles of incidence. In Fig. 7 a constant solid angle is assumed, so that each angle represents a solar panel with a different area.

Figure 7 shows the angular dependence of J_{sc} for both the light-trapping structure and the reference cell. Contrary to what one might assume, the average J_{sc} increases with incidence angle for both cell structures. For the light-trapping cell J_{sc} is notably higher at angles around 10 - 20 degrees than at normal incidence, before it starts to drop steadily cell for higher θ. The reference cell has a smaller J_{sc} increase at small θ, but it lasts all the way to 55 degrees.

#119649 - $15.00 USD Received 6 Nov 2009; revised 24 Feb 2010; accepted 24 Feb 2010; published 3 Mar 2010

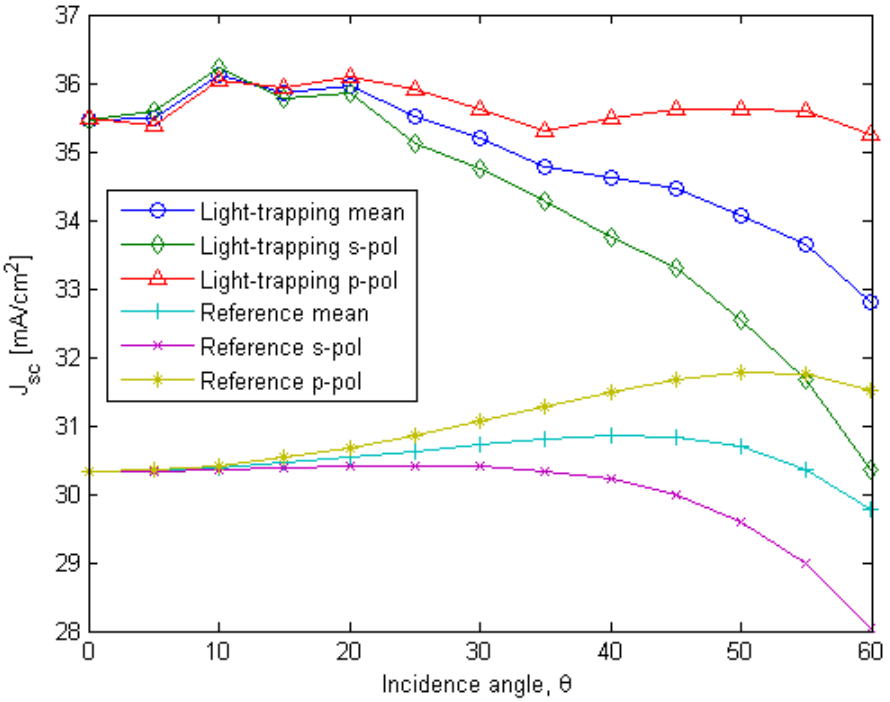

Fig. 7. The figure shows the effect of incidence angle on J_{sc} for the cell with light-trapping structure and for the reference cell. Both p-polarization and s-polarization and their mean are shown.

The increase in J_{sc} for the reference cell can be explained by the Brewster angle effect, where front-side reflectance will be reduced towards zero for p-polarization. The light-trapping cell will experience the same Brewster angle effect at the front surface. However, the improvement in J_{sc} is more than what would be expected from this effect at small θ while J_{sc} is significantly lower where the Brewster effect is at its strongest. An increase in J_{sc} at small θ was also reported in [17] for a 1D line grating. We believe this increase might be attributed to less out-coupling of light due to the reduced symmetry at oblique incidence. The problem of out-coupling is discussed in [6].

Varying the incidence angle θ_i in the grating equation (i.e. Eq. (2)) will also change the angles of the outgoing modes in the same plane. By inserting $\bar{\lambda}$ from Eq. (3) into Eq. (2) we find that at an incidence angle $\theta_i = 23.5$ degrees, the m = −1 mode (in the same plane) will no longer be totally internally reflected at the front surface. This gradual escape of diffraction orders is an effect which may explain parts of the reduction in J_{sc} that we observe for the light-trapping structure.

5. Discussion

Due to the recent advances in crystalline Si substrate manufacture described above, we have chosen to focus our attention on Si cells with a thickness of 20 µm. This is considerably thinner than state of the art wafer-based cells today (around 160 µm), but also well above the common thin-film technologies with layer thickness of only a few microns. The relative gain by adding a light trapping structure will of course be larger the thinner the cell, and most of the earlier works focus on cells significantly thinner than 20 µm. However, an advantage of the semi-thin (e.g. 20 µm) cells investigated in this work is that the spectrum of the light that is transmitted to the back side is narrower than for thinner cells, due to significantly stronger

#119649 - $15.00 USD Received 6 Nov 2009; revised 24 Feb 2010; accepted 24 Feb 2010; published 3 Mar 2010

absorption at shorter wavelengths. It is therefore possible to optimize the light trapping effect for the narrow spectral range that reaches the back side of the 20 μm thick Si-slab. Periodic structures are particularly well suited for this purpose, since they can easily be exploited to make a narrowband trapping response.

In general, the parasitic absorption in a metal mirror is higher, the higher the index of refraction is in the adjacent dielectric where the light propagates. The SiO_2-Al boundary reduces parasitic absorption of light in the metal compared to a Si-Al boundary. Another vital effect of the SiO_2-layer is to move the metal away from the grating, so that the evanescent waves from the grating that reach the metal are weaker. As we saw in Table 1, Ag may help to further reduce the parasitic absorption. However, the improvement of 1.1% by replacing the Al mirror with Ag is not as large as one would expect by looking at the reflecting properties of the two materials. The reason for this we believe to be that our structure is optimized both for light scattering and for reduced absorption, thus maximizing J_{sc}. We should point out that we have just simulated the performance of an Ag mirror used with a grating structure optimized for an Al mirror; we have not optimized the grating structure for an Ag mirror. The advantages of using Al as a back reflector instead of Ag are not just the material costs, but also that Al is directly compatible with the laser fired contact process [33], which is one obvious way of making the electrical contact at the back side of the cell.

We have focused in this work on binary cylindrical geometries with oxide cylinders in silicon as shown in Fig. 1. Binary structures have the advantage of requiring relatively short computation times with RCWA compared to more complex geometries. In addition they may be fabricated using conventional silicon micro-fabrication technology. The simplicity of such a binary system is also favorable for analyzing the interactions between light and the grating structure. Other geometries may possibly hold the potential for even more efficient light trapping. For example, it has been shown that blazed gratings perform better than binary gratings for a 1D structure when the grating structure was applied to both the front and the back side [6,18].

We have investigated different cylinder configurations; triangular lattice instead of square, and silicon cylinders instead of oxide cylinders. We found no significant difference in the maximum J_{sc} between the different configurations. We have found that a SiO_2 fill-factor above 0.5 (i.e., oxide cylinders with radius above 0.4Λ or Si cylinder with radius below 0.4Λ) is favorable for silicon cylinders as well as for oxide cylinders. On the other hand, Fig. 5 shows that there is a wide range of different periods and fill factor combinations that have the potential of providing a high J_{sc}. This freedom in design with respect to period, fill factor and material may be an advantage with respect to fabrication.

To further increase the light trapping a better AR-coating is needed. A double layer AR-coating would add more than 1 mA/cm^2 to all the J_{sc}-values of Table 1. Encapsulating the cell would also help reduce the front side reflectance by making the change in refractive index more gradual. To reduce the reflectance further, a front-side texturing of some sort is usually applied. Configurations with a 1D front and back-side periodic grating have been shown to increase light trapping compared to configurations with only a 1D back-side grating [11,17]. The effect of a randomly structured front side, however, is difficult to assess. Simulation of random structures with the RCWA method are very slow, because they are typically done with the help of very large unit cells that are many wavelengths on the side, but with adequate resolution to resolve the periodic structures.

6. Conclusion

We have presented a light-trapping design for a solar cell, incorporating a back-side bi-periodic pattern of silica (SiO_2) cylinders combined with a layer of SiO_2 to detach the grating from the back-side Al mirror. The grating increases the coupling of light into the Si solar cell, while the layer of SiO_2 reduces the parasitic absorption in the Al mirror and ensures a good surface passivation. Simple design criteria for optimizing grating performance have been presented. In particular the interaction between the EM-waves in the grating layer and oxide layer has been investigated for two extreme cases (i.e. large periods and short periods),

#119649 - $15.00 USD Received 6 Nov 2009; revised 24 Feb 2010; accepted 24 Feb 2010; published 3 Mar 2010

showing good agreement between fully vectorial EM-field simulation results and simple scalar optical field models. The scalar models are very helpful in limiting the parameter space for the numerical simulations. We have performed numerical simulations to quantify the light trapping in terms of the short circuit current density. Our simulations show that for an optimized 20 μm thick Si solar cell, a short circuit current density of 35.5 mA/cm^2 would be obtained if all the charge carriers are collected at the contacts. This is an increase of more than 17% compared to a reference cell with the same thickness and a planar back-side Al mirror. Our design is also effective for thinner cells, and we see an improvement compared to two recently published papers for cell thicknesses of 2 and 5 μm, respectively. The light-trapping design presented shows promising behavior over a wide range of incidence angles. To further improve the light trapping, the front-side reflection should be reduced.

Acknowledgments

The author acknowledges the Nordic Center of Excellence in PV and the Norwegian Research Council through the Nanomat program for the financial support.

#119649 - $15.00 USD Received 6 Nov 2009; revised 24 Feb 2010; accepted 24 Feb 2010; published 3 Mar 2010